



**HAL**  
open science

## Experimental and numerical study of the influence of the PP fiber diameter on spalling behaviour of concrete

Fariza Sultangaliyeva, Chhainan Leang, H el ene Carr e, Christian La Borderie,  
Nicolas Roussel

### ► To cite this version:

Fariza Sultangaliyeva, Chhainan Leang, H el ene Carr e, Christian La Borderie, Nicolas Roussel. Experimental and numerical study of the influence of the PP fiber diameter on spalling behaviour of concrete. 6TH INTERNATIONAL WORKSHOP ON CONCRETE SPALLING DUE TO FIRE EXPOSURE, Sep 2019, Sheffield, United Kingdom. hal-02946254

**HAL Id: hal-02946254**

**<https://hal.science/hal-02946254v1>**

Submitted on 23 Sep 2020

**HAL** is a multi-disciplinary open access archive for the deposit and dissemination of scientific research documents, whether they are published or not. The documents may come from teaching and research institutions in France or abroad, or from public or private research centers.

L'archive ouverte pluridisciplinaire **HAL**, est destin ee au d ep ot et  a la diffusion de documents scientifiques de niveau recherche, publi es ou non,  emanant des  tablissements d'enseignement et de recherche fran ais ou  trangers, des laboratoires publics ou priv es.

# Experimental and numerical study of the influence of the PP fiber diameter on spalling behaviour of concrete

Fariza Sultangaliyeva<sup>1\*</sup>, Chhainan Leang<sup>2</sup>, H  l  ne Carr  <sup>1</sup>, Christian La Borderie<sup>1</sup>, Nicolas Roussel<sup>3</sup>

<sup>1</sup> SIAME, Universit   de Pau et des Pays de l'Adour, Anglet, France

<sup>2</sup> INSA Rennes, Rennes, France

<sup>3</sup> IFSTTAR, Champs-sur-Marne, France

\* Corresponding author ([fariza.sultangaliyeva@univ-pau.fr](mailto:fariza.sultangaliyeva@univ-pau.fr),  
1 All  e du Parc Montaury, 64600 Anglet, France)

## ABSTRACT

In this work, the influence of diameter of polypropylene (PP) fiber on the spalling of concrete was studied. Concrete prisms of 20 x 20 x 10 cm<sup>3</sup> containing 2 different diameters of fibers (32 and 20   m) were tested under ISO 834-1 fire curve. In addition to this, tests of residual radial permeability to nitrogen were performed for the same mixes after heating to 80, 150 and 200   C. Following this, numerical simulations using thermo-mechanical model were performed in order to investigate the influence of the PP fiber diameter on the damage behaviour of cementitious materials. The expansion of fibers during heating can be sufficient for a formation of cracks around the fibers which can increase the permeability and then reduce the risk of concrete instability. The simulations are performed using finite-element code developed in Cast3M. The work carried out made it possible to investigate the influence of PP fiber diameter on the concrete exposed to a high temperature.

**KEYWORD:** Polypropylene Fiber, Damage, Fiber Diameter, Fire Tests, Simulation.

## INTRODUCTION

Polypropylene fibers are used to counteract the thermo-hydric mechanism of spalling through the increase of the permeability of heated concrete by creation of additional vapor channels when polypropylene is melted. Current literature presents the influence of the PP fiber diameter for the same volume of fibers. Consequently, for the same fiber volume slender fibers have a higher number of fibers compared to thicker ones. For example, in [1] 28   m fibers had the highest increase in permeability compared to 32   m fibers (L= 6mm). For the same fiber volume the number of fibers was 3.2 times higher for slender fibers. In [2], addition of 0.68 kg/m<sup>3</sup> of 18   m fibers was as effective as 1.2 kg/m<sup>3</sup> of 32   m fiber in terms of spalling prevention. Knack [3] has concluded on the efficiency of a finer cross section of fibers over a larger one based on the total number of fibers. In [4], samples containing two fiber diameters of 20 and 40   m at the same number of fibers were tested for spalling extent. It was noted that regardless a diameter, when 133/cm<sup>3</sup> was reached, spalling was prevented.

In this study, the influence of PP fiber is evaluated using fire tests on concrete prisms and residual radial permeability tests to nitrogen on hollow cylinders. Two fiber diameters were studied at two fiber dosages that were fixed to same total number (and total length)

of fibers. To complete the study, numerical simulations of PP fiber were conducted as well.

## EXPERIMENTAL STUDY

### Concrete mixes

Concrete samples with  $w/c=0.4$  were prepared using cement CEM III/A 52.5 L CE from Eqiom, Heming. The contents of clinker and of ground granulated furnace slag were 35 and 61 % respectively. The information about the concrete mixes is presented in Table 1. The aggregate skeleton constitutes of 60% of siliceous sand 0/1 and 40% of calcareous gravel 6.3/10. A size of the gravel 6.3/10 was obtained through screening and sieving of gravel 4/10. The aggregates were dried in oven at 80 °C for 24 hours and cooled to a room temperature prior to casting. PP fibers used in this study were monofilament polypropylene fibers from Baumhüter. Two fiber geometries  $L = 12 \text{ mm}$ ,  $D = 32 \mu\text{m}$  and  $L = 12\text{mm}$ ,  $D = 20 \mu\text{m}$  were used. Fiber dosages were fixed to obtain the same total length (and total number), i.e. 683 and 1366  $\text{km}/\text{m}^3$ . Therefore, for fibers of 12/32 (L/D) this has resulted in two fiber dosages of 0.50 and 1.00  $\text{kg}/\text{m}^3$ , while for 12/20 fibers- in 0.20 and 0.39  $\text{kg}/\text{m}^3$ .

The example of the mix reading (see Table 1): C1-12/20-0.2 stands for concrete with PP fibers of length of 12 mm and diameter of 20  $\mu\text{m}$  with a dosage of 0.20  $\text{kg}/\text{m}^3$ .

Table 1 Information about concrete mixes studied\*.

	Unity	C1-0	C1-12/32-0.5	C1-12/32-1	C1-12/20-0.2	C1-12/20-0.4
Cement CEM III/A 52.5 - Eqiom	$\text{kg}/\text{m}^3$			500		
Water	$\text{kg}/\text{m}^3$			200		
Siliceous filler - Sibelco	$\text{kg}/\text{m}^3$			120		
Siliceous sand 0/1 - Messanges	$\text{kg}/\text{m}^3$			623		
Gravel 6.3/10 - Sare	$\text{kg}/\text{m}^3$			945		
PP fibers 12/32 - Baumhüter	$\text{kg}/\text{m}^3$		0.50	1.00		
PP fibers 12/20 - Baumhüter	$\text{kg}/\text{m}^3$				0.20	0.39
SP - SIKA Krono 26	$\text{kg}/\text{m}^3$			3.75		
w/c ratio	-			0.4		
Slump flow	mm	809	830	792	843	764
$f_{c,cyl}$ at 28 days	MPa			90.1 ± 5.3		
Water content	%	4.24	5.14	5.40	5.23	4.40

\* The expressed values are theoretical, the real density of fresh concrete was not taken into account.

The samples were cast and demolded after 24 hours and placed in the water for 59 days. The compressive strength was measured on three cylinders 11 x 22  $\text{cm}^2$  of C1-0 only.

### Fire test

The fire tests were conducted using gas furnace (see Figure 1) on loaded prismatic samples of 20 x 20 x 10  $\text{cm}^3$ . All the samples were tested in water saturation condition. The fire curve was the standard fire curve ISO 834-1 with a duration of 30 minutes. Temperature was tracked by three K-type thermocouples installed 1 cm from heated face and 4, 10 and 16 cm from the bottom of the furnace opening (see Figure 1). A uniaxial loading of 5 MPa was applied before test and maintained throughout the test. One face of the sample was heated, area exposed to fire was 20 x 20  $\text{cm}^2$ . The lateral sides of the sample were insulated with aluminium foil glued with a high temperature resistant glue.

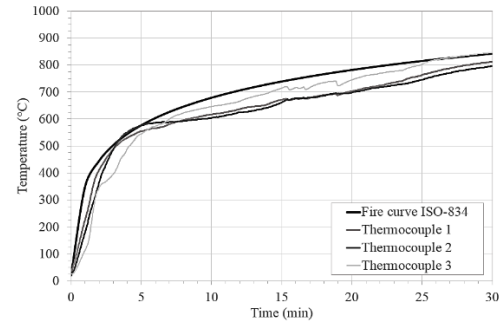
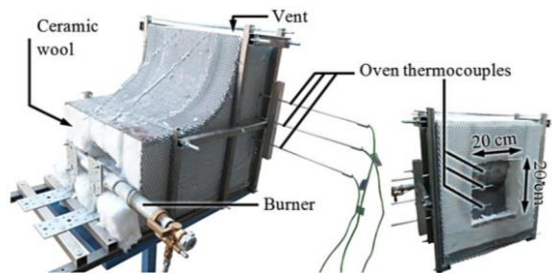


Figure 1 Gas furnace [5] and ISO 834-1 followed by thermocouples.

The sample was placed between two fiber-reinforced concrete samples for mechanical load distribution. The sides of the setup were insulated by 12 cm of rock wool. The opening of the gas furnace was located in front the sample and gas was burned. When the test was finished, the spalling depth of the sample was measured by means of photogrammetry. The error from photogrammetry is calculated to be 4.2 %.

### Residual radial permeability to nitrogen

Residual radial permeability to nitrogen was performed after heating-cooling cycle on hollow cylinders. The samples were double cored from cubes of  $15 \times 15 \times 15 \text{ cm}^3$ . Top and bottom surfaces were grinded to ensure flatness and parallelism. Dimensions of the final sample are: outer and inner radius  $R_1$  and  $R_2$  of 5.50 and 2.85 cm accordingly with a height of 14 cm. Before start of the test, the samples were dried at  $80^\circ\text{C}$  until mass stabilization. The sample is considered dry when the difference between the two consecutive daily mass loss measurements is less than or equal to 0.02% of the mass of the dry sample. Drying of samples was accomplished in order to evaporate free water without provoking a change in the microstructure.

The measurements are performed on the cooled samples that were heated to 80, 150 and  $200^\circ\text{C}$ . The heating rate of the samples was fixed to  $1^\circ\text{C}/\text{min}$  in order to avoid creation of significant thermal stresses. After reaching a required temperature, the stabilization time of 3 hours was set to ensure uniformity of temperature across the sample. Cooling of samples was performed in the furnace with an estimated rate of  $1^\circ\text{C}/\text{min}$ .

The setup for the measurement of the radial permeability is shown in Figure 2. Before each permeability test, steel inox plates were glued on the top and on the bottom surfaces of the sample to prevent gas leakage. The bottom plate has a borehole to which a connector for the gas flow with a tube are fixed. The sample with metal plates is placed on the top of the support sample. A support sample is a hollow cylinder  $11 \times 22 \text{ cm}^2$  that is used to pass the tube that supplies gas. The test sample and the support sample are placed between two plates of press. A constant uniaxial compressive load is applied in order to counteract the injection pressure.

Nitrogen is injected with injection pressure  $P_i$  through the borehole. The flow rate of gas is measured using the mass flow meters that is then converted into volume flow rate. Depending on the flow rate, the flow meter for the measurement is selected. Pressure and temperature are recorded. The flow rate is recorded when the gas flow stabilization is achieved. Then, another injection pressure is applied and the same procedure is repeated. In this study a steady-state flow of the gas is considered.

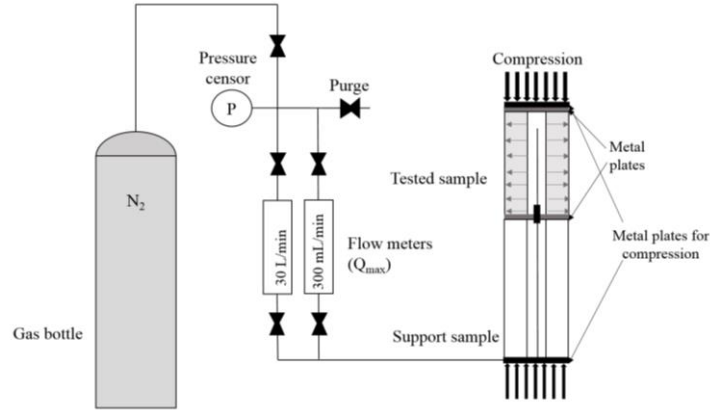


Figure 2 Schematic representation of radial permeability setup.

We can then compute the apparent permeability  $K_a$  ( $m^2$ ) derived from Darcy's law for the laminar flow of compressible gas [6] using Eq.(1).

$$K_a = \frac{Q_i P_i \mu \ln\left(\frac{R_1}{R_2}\right)}{\pi H (P_i^2 - P_{atm}^2)} \quad (1)$$

where  $Q_i$  is the flow rate ( $m^3/s$ ),  $P_i$  is the injection pressure (Pa),  $\mu$  is the dynamic viscosity of gas (Pa.s),  $R_1$  is the outer radius of the sample (m),  $R_2$  is the inner radius of the sample (m),  $H$  is the sample height (m),  $P_{atm}$  is the atmospheric pressure (Pa).

We compute intrinsic permeability of the material  $K_i$  ( $m^2$ ) by using Klinkenberg's method (see Eq.(2)) that would allow considering viscous flow only [7].

$$K_a = K_i \left(1 + \frac{\beta}{P_m}\right) \quad (2)$$

where  $\beta$  is Klinkenberg's coefficient,  $P_m$  is mean pressure. The mean pressure is computed as  $P_m = (P_i + P_{atm})/2$ .

We measure radial permeability at five different injection pressures: 1, 1.5, 2, 2.5 and 3 bars. The values of apparent permeability are plotted as a function of mean inverse pressure  $1/P_m$ . The intrinsic permeability is then found at the intersection of the line traced from apparent permeability measurements done at various injection pressures with apparent permeability axis.

## EXPERIMENTAL RESULTS

### Fire tests results

The results for the spalling tests such as mean, maximum spalling depth as well as spalled volume were obtained by the means of photogrammetry. A linear relationship between mean spalling depth, maximum spalling depth and spalled volume was observed; therefore, in Figure 3 we present mean spalling depth results only. It should be noted that for the same total length of fibers we have the same total number of fibers as the fiber length is 12 mm. For each of the mix three samples were tested. The average values are shown with a cross sign.

For non-fibred samples C1-0, mean spalling depth varied between 0.23 and 1.61 cm with an average value of 1.04 cm. As fiber dosage was increased from 0 to  $0.5 \text{ kg/m}^3$  for samples C1-12/32-0.5 and from 0 to  $0.2 \text{ kg/m}^3$  for samples C1-12/20-0.2 resulting in total

fiber length of 686 km/ m<sup>3</sup>, mean spalling depth has decreased for both materials to 0.26 and 0.58 cm respectively.

An increase of the dosage from 0.5 kg/m<sup>3</sup> and 1 kg/m<sup>3</sup> had almost no effect for concrete with 32 μm PP fibers. However, for 20 μm fibers mean spalling depth has decreased passing from 0.2 to 0.4 kg/m<sup>3</sup>. It is interesting to note that at the total length of fibers of 1366 km/m<sup>3</sup> the values for mean spalling depth for both 32 μm and 12 μm PP fibers almost coincide. The results show that at lower dosage larger fibers are more efficient than thinner ones. However, as we increase the dosage, almost no difference in terms of the influence of fiber diameter on spalling is observed.

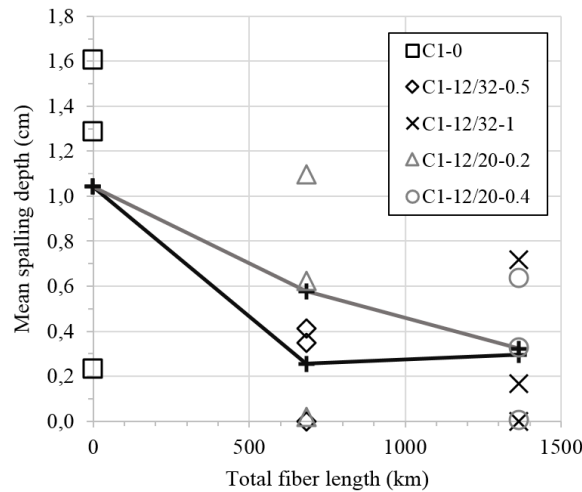


Figure 3 Mean spalling depth for tested concrete mixes.

### Residual permeability results

The evolution of the intrinsic permeability with a temperature was obtained for all concrete mixes (see Figure 4). Two samples were tested for each mix. The values presented are the average ones, the error bar gives the range of the data. The maximum total error including the measurement error and eccentricity error due to coring is 4%. All the values of the intrinsic permeability for non-fibred and fibrous materials are low, the order of values is 10<sup>-17</sup>-10<sup>-18</sup> m<sup>2</sup>.

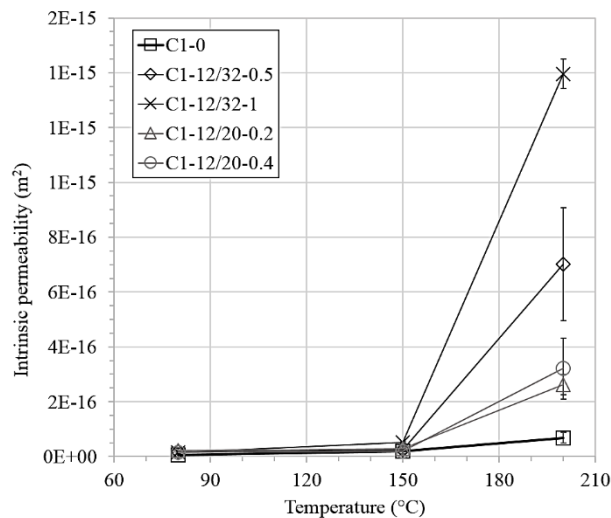


Figure 4 Intrinsic permeability evolution with temperature for tested concrete mixes.

Figure 4 shows an increase of the intrinsic permeability of concrete with the temperature. The increase of the permeability between 80 and 150 °C is 4.4 times for non-fibred C1-0 and 1.3 to 3.5 times for fibrous mixes. At 150 °C, PP fibers have not melted yet, thus, no substantial increase in the permeability should be observed. In [8], a significant increase of the permeability is observed starting 130 °C even before the melting of PP fibers. The authors have explained this phenomena by the loss of the thermal stability of polypropylene that creates the cavities between matrix and fiber before its melting. In [9], the increase of the permeability was linked to cracking caused by a high difference of linear coefficients of thermal expansion of concrete and polypropylene.

From Figure 4 at 200 °C, significant increase in the intrinsic permeability for all the materials is observed. A part of the increase of the permeability is attributed to the thermal mismatch between aggregates and cement paste. Starting from 150 °C, a dehydration of cement paste causes its shrinkage whereas aggregates constantly expand [10]. For fiber reinforced materials, drastic increase of the intrinsic permeability is noted. For concrete with 32 µm fibers there is a remarkable increase of the permeability with the increase of the dosage of PP fiber: 40 and 952 times the initial permeability for 0.5 and 1 kg/m<sup>3</sup> of fibers. For the concrete with 20 µm fibers, the increase of the permeability is less significant: 12 and 18 times the initial permeability for dosages of 0.2 and 0.4 kg/m<sup>3</sup>.

The dosage of 0.5 kg/m<sup>3</sup> of 32 µm fibers was efficient for a significant reduction of spalling extent compared to 0.2 kg/m<sup>3</sup> of 20 µm fibers. This is linked to the fact that 32 µm fibers provoke a higher increase in the permeability compared to 20 µm fibers. The results show that for fully saturated concrete samples, the beneficial influence of PP fibers in terms of permeability increase is not sufficient for total elimination of spalling phenomenon.

## NUMERICAL STUDY

### Material properties

- Polypropylene

PP fibers are used for a prevention of concrete spalling due to fire based on their ability to melt at relatively low temperature, to flow into cracks and pores and to leave the empty channels that serve for vapor escape. In general, melting of PP starts at 150 °C, peaks at 165 °C and ends around 176 °C [11]. During that stage, PP, a semi-crystalline material, undergoes a phase change: its crystalline phase is destroyed and turned into amorphous one. Mechanical properties of polymers are linked to the crystallinity, the destruction of latter will lead to the decrease in former. PP has an elastic modulus of 1100 MPa at 20 °C as seen in Figure 5A [12]. As material is heated, it's elastic modulus decreases and eventually drops to zero at the melted state.

PP as a bulk material is isotropic. Manufacturing process of PP fibers (extrusion and injection molding) imposes anisotropy on fibers. When fibres are heated, the energy introduced into the system releases the imposed stresses and allows for the rearrangement of molecules in the preferential orientation leading to anisotropic volume change. This change is characterized by the contraction in length and expansion in thickness. At 20 °C the density of PP is 910 kg/m<sup>3</sup> and in melted state - 850 kg/m<sup>3</sup> [11, 12] resulting in 7 % volume expansion [11]. It is important to precise that in our calculations we consider isotropic behaviour of fibers. The evolution of the coefficient of thermal expansion (CTE) of PP is presented in Figure 5B [14]. Similar values are observed in [13], where the linear CTE for PP is given as  $1 \times 10^{-5} / ^\circ\text{C}$  for  $T = 20 - 60$  °C,  $15 \times 10^{-5} / ^\circ\text{C}$  for  $T = 60 - 100$  °C and  $21 \times 10^{-5} / ^\circ\text{C}$  for  $T = 100 - 140$  °C. In Figure 5B [14],

the CTE of PP skyrockets around 160 °C due to expansion linked to phase transition. When polypropylene has melted, the shrinkage due to thermal contraction as well as the compressibility of the melted material occurs.

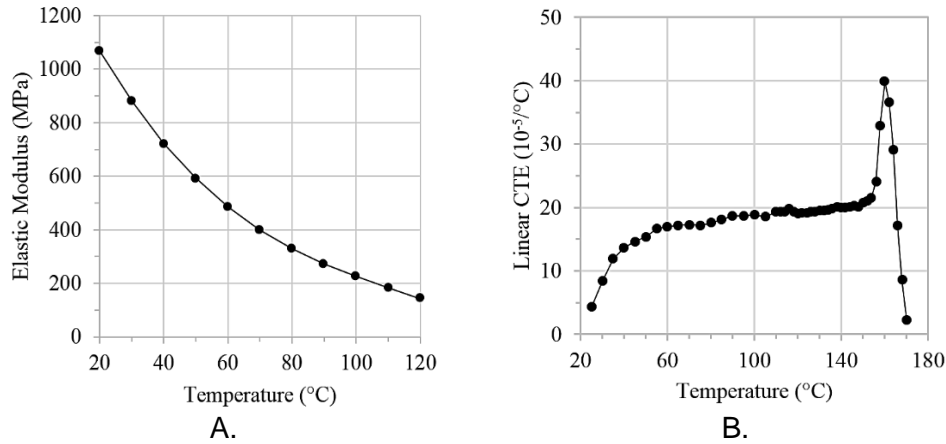


Figure 5 Evolution of the properties of polypropylene with temperature (A): elastic modulus (adapted from [12]), (B): linear coefficient of thermal expansion with temperature for polypropylene (adapted from [14])

Poisson ratio of polypropylene at 20 °C is 0.42 [12]. As polypropylene passes from the semi-crystalline material to completely amorphous rubbery material, our hypothesis is that its Poisson's ratio is close to the rubber (=0.49) in melted state.

- Mortar

Experimentally determined evolution of mortar properties with a temperature is presented in Table 2. Poisson's ratio is considered constant (= 0.2).

Table 2 Evolution of density, CTE, elastic modulus, tensile strength, fracture energy with temperature for mortar.

Temperature (°C)	Density (kg/m <sup>3</sup> )	CTE (10 <sup>-5</sup> /°C)	Elastic modulus (MPa)	Tensile strength (MPa)	Fracture energy (J/m <sup>2</sup> )
20	2300	1	15	4	40
120	2297	1.3	10	3.2	47
250	2254	1.5	10	3.48	69
400	2185	1.5	6	3.36	71
600	2145	1.5	2	2.4	122

### Numerical model

Thermo-mechanical (TM) computations are accomplished in Cast3M. In terms of thermal conditions, the evolution of the temperature is imposed, no heat transfer is performed. For mechanical model, an improved elasto-plastic damage model named 'microiso' is used. This computational model is based on the continuum damage mechanics of [15] and takes into account fracture energy [16].

From continuum mechanics, the relationship between total stress and effective stress is:

$$\tilde{\sigma}_{ij} = C_{ijkl}^0 \varepsilon_{kl} = C_{ijkl}^0 (C^{endom})_{klmn}^{-1} \sigma_{mn} \quad (3)$$

where  $\tilde{\sigma}_{ij}$  is effective stress,  $\sigma$  is total stress,  $C_{ijkl}^0$  is rigidity of undamaged material,

$C_{ijkl}^{endom}$  is rigidity of damaged material.

An evolution law for damage variable is determined [16]:

$$d = 1 - \frac{\varepsilon_{d0}}{\varepsilon} \exp [B(\varepsilon_{d0} - \varepsilon)] \quad (4)$$

where  $\varepsilon_{d0}$  is threshold for damage,  $\varepsilon$  is deformation and  $B$  is slope of softening curve defined by exponential expression.

Damage threshold is computed as:

$$\varepsilon_{d0} = \frac{f_t}{E} \quad (5)$$

where  $f_t$  is tensile strength,  $E$  is elastic modulus.

Evolution parameter  $B$  is given as:

$$B = \frac{f_t}{G_f} \quad (6)$$

where  $G_f$  is fracture energy.

3D TM calculations on the quarter of the cylinder were accomplished. Fiber was placed in the center, radius of concrete modelled around the fiber was 1 mm. The displacement of the upper face of the quarter of the cylinder is equal for both fiber and mortar. This does not correspond neither to plain stresses nor to plain strains. For this reason, 3D calculations were completed.

## NUMERICAL RESULTS

Two fiber diameters were modelled: 20 and 32  $\mu\text{m}$ . Temperature was increased from 20 to 220  $^{\circ}\text{C}$ . The results of the damage of mortar (damage is greater than 0.94) at 220  $^{\circ}\text{C}$  for two fiber diameters are presented in Figure 6. The results show that damage radius increases with the diameter of the fiber. To compare, at 220  $^{\circ}\text{C}$ , damage radius for mortar with 32  $\mu\text{m}$  fiber is 40  $\mu\text{m}$  compared to 24  $\mu\text{m}$  for 20  $\mu\text{m}$  fiber.

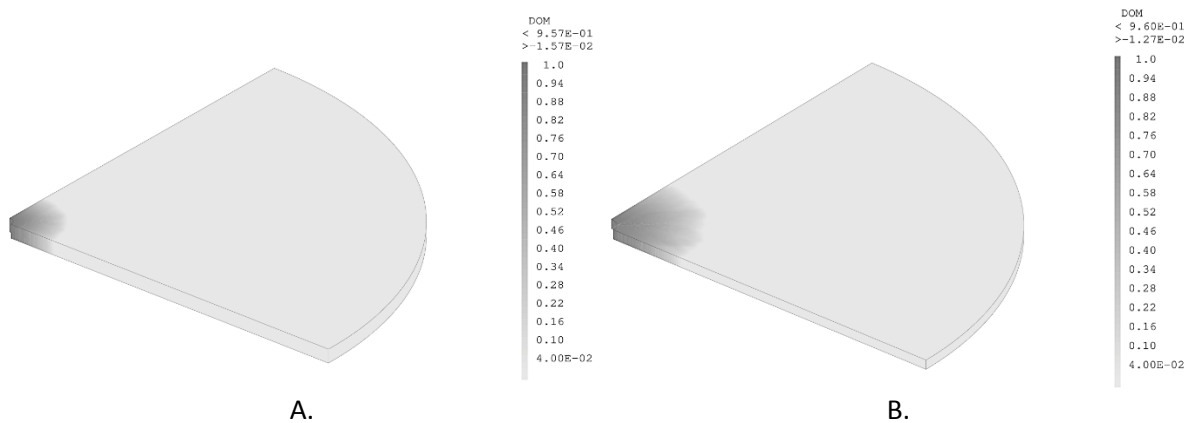


Figure 6 Damage of mortar at 220  $^{\circ}\text{C}$  for fiber diameter (A):  $D = 20 \mu\text{m}$ , (B)  $D = 32 \mu\text{m}$ .

In Figure 7, the evolution of the damage radius with temperature for 20  $\mu\text{m}$  and 32  $\mu\text{m}$  fibers is shown. First, it is notable that the damage increases with temperature. A slight damage appears at 45  $^{\circ}\text{C}$  and its value increases till 115  $^{\circ}\text{C}$ . Thermal deformations occur due to the increase of the CTE of polypropylene with temperature. Then, no evolution of damage is

observed between 110 and 155 °C. A sudden increase of the damage radius at 155 °C is linked to the expansion of the fibre provoked by its phase change. After this temperature, the value of the CTE of polypropylene decreases and no evolution of damage is observed. The results contradict the findings in [9], which observe the cracking appear at 105 °C.

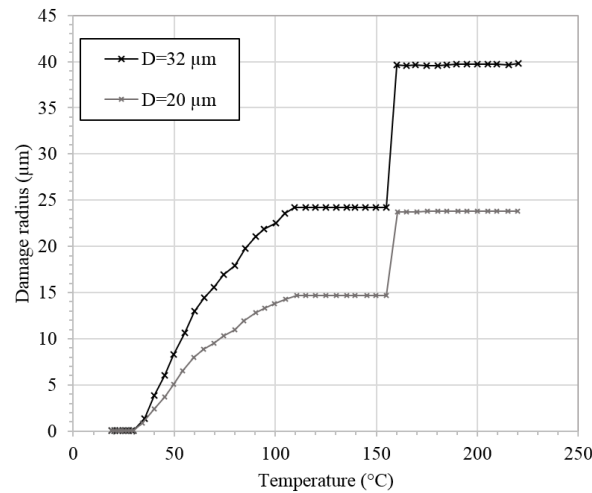


Figure 7 Evolution of the mortar damage radius with temperature for two fiber diameters.

## DISCUSSION

Experimental and numerical studies show the existence of the effect of the PP fiber diameter on the behaviour of the fiber-reinforced concrete at high-temperature. From spalling tests on water saturated samples, at dosage of 0.5 kg/m<sup>3</sup> efficiency of 32 μm fibers over fibers of 0.2 kg/m<sup>3</sup> of 20 μm is observed. At 0.4 kg/m<sup>3</sup>, spalling depth for 20 μm decreases but for 32 μm fibers at 1 kg/m<sup>3</sup> remains the same as at 0.5 kg/m<sup>3</sup>. Permeability tests show that concrete with 32 μm fibers has a higher permeability compared to concrete with 20 μm fibers. From numerical simulations, it is clear that fibers can induce damage due to a high CTE at temperatures close to their melting point. The damage zone increases with temperature and reaches its maximum value during phase transition. Calculations show that damage radius increases with fiber diameter.

Permeability increases significantly with damage of the material [6]. Therefore, at high temperature expansion of larger fibers introduces damage that affects a larger zone around the fiber which improves percolation of cracks and pores leading to a higher increase of permeability. Consequently, increase of permeability may lead to pore pressure drop and reduction of spalling.

## CONCLUSIONS

In this paper, we have examined the influence of PP fiber on the behaviour of concrete at high temperature. Two fiber diameters were examined (20 and 32 μm), the dosage of fibers was fixed to obtain the same total number and total length (fiber lengths are the same: 12 mm). Fire tests performed on water saturated samples show that at dosage of 0.5 kg/m<sup>3</sup>, fibers of 32 μm are more efficient than 20 μm. Residual radial permeability tests show a significant increase for 32 μm fiber compared to 20 μm for two fiber dosages. The results are explained by numerical simulations that show that the damage radius around the fiber increases with fiber diameter. The damage zone increase induces improved percolation, higher permeability and reduced spalling risk.

## ACKNOWLEDGEMENTS

The authors would like to acknowledge that this work is carried out using the financial assistance from the program of the Investments for the Future of the French government managed by ANDRA.

## REFERENCES

1. Lu, F. and Fontana, M, "Effects of Polypropylene Fibers on Preventing Concrete Spalling in Fire", Proceedings of the 9<sup>th</sup> International Conference on Structure in Fire SiF' 16, Princeton, USA, 8-10 June, 2016.
2. Maluk, C., Bisby, L. and Terrasi, G. P., "Effects of polypropylene fibre type and dose on the propensity for heat-induced concrete spalling", *Engineering Structures*, **41**, 584-595, 2017.
3. Knack, I., "New pp-fibre with exceptional melting characteristics for improved fire protection in concrete building", Proceedings of the 1<sup>st</sup> International Workshop on Concrete Spalling due to Fire Exposure, 238-247, Leipzig, Germany, 3-5 September, 2009.
4. Heo, Y.-S., Sanjayan, J.G., Han, C-G., Han, M.-C., " Limited effect of diameter of fibres on spalling protection of concrete in fire", *Materials and Structures*, **45**, 325-335, 2012.
5. Miah, Md. J., Carré, H., Pimienta, P., Pinoteau, N. and La Borderie, C., "Effect of uniaxial mechanical loading on fire spalling of concrete", Proceedings of the 4<sup>th</sup> International Workshop on Concrete Spalling due to Fire Exposure, 124-131, Leipzig, Germany, 8-9 October, 2015.
6. Choinska, M., "Effets de la température, du chargement mécanique et de leurs interactions sur la perméabilité du béton de structure" (in French), PhD Thesis, Ecole Centrale de Nantes et l'Université de Nantes, Nantes, France, 2014.
7. Klinkenberg, L.J., "The permeability of porous media to liquid and gases", *Drilling and Production Practice*, 200-213, 1941.
8. Bošnjak, J., Ožbolt, J., Hahn, R., " Permeability measurement on high strength concrete without and with polypropylene fibers at elevated temperatures using a new test setup", *Cement and Concrete Research*, **53**, 104-111, 2013.
9. Zhang, D., Dasari, A., Tan, K.H., "On the mechanism of prevention of explosive spalling in ultra-high performance concrete with polymer fibers", *Cement and Concrete Research*, **113**, 169-177, 2018.
10. Bazant, Z.P. and Kaplan, M.F., "Concrete at High Temperatures: Material Properties and Mathematical Models", Pearson Education, 1996.
11. Khoury, G.A., and Willoughby, B., "Polypropylene fibres in heated concrete. Part I: Molecular structure and materials behaviour", *Magazine of Concrete Research*, **60**, 125-136, 2008.
12. Maier, C., and Calafut, T., "Polypropylene: The Definitive User's Guide and Databook", William Andrew, 1998.
13. Tripathi, D, "Practical Guide to Polypropylene", Smithers Rapra, Shrewsbury, United Kingdom Publishing, 2002.
14. Kanapitsas, A., Tsonos, C., Pandis, C., Pissis, P., Kontou, E., Mamunya, Y.P., Lebedev, E.V. and Delides, C.G., " PTC Effect and Structure of Polymer Composites Based on Polypropylene/Co-Polyamide Blend Filled with Dispersed Iron", Proceedings of the 25<sup>th</sup> International Conference on microelectronics, Belgrade, Serbia and Montenegro, 14-17 May, 2006.
15. Fichant, S., La Borderie, C. and Pjaudier-Cabot, G., "Isotropic and anisotropic description of damage in concrete structures", *Mechanics of Cohesive-frictional Materials*, **4**, 339-359, 1999.
16. Matallah, M., La Borderie, C. and Maurel, O., "A practical method to estimate crack openings in concrete structures", *International Journal for Numerical and Analytical Methods in Geomechanics*, **34**, 1615- 1633, 2010.